OPEN ACCESS
IOP Publishing
Journal of Physics: Condensed Matter
J. Phys.: Condens. Matter **36** (2024) 255802 (8pp)
https://doi.org/10.1088/1361-648X/ad3473

Robust magnetism and crystal structure in Dirac semimetal $EuMnBi_2$ under high pressure

Greeshma C Jose[1], Weiwei Xie[2], Barbara Lavina[3,4], Jiyong Zhao[3], Esen E Alp[3], Dongzhou Zhang[5] and Wenli Bi[1,*]

[1] Department of Physics, University of Alabama at Birmingham, Birmingham, AL 35294, United States of America
[2] Department of Chemistry, Michigan State University, East Lansing, MI 48824, United States of America
[3] Advanced Photon Source, Argonne National Laboratory, Argonne, IL 60439, United States of America
[4] Center for Advanced Radiation Sources, The University of Chicago, Chicago, IL 60637, United States of America
[5] Hawaii Institute of Geophysics and Planetology, School of Ocean and Earth Science and Technology, University of Hawaii at Manoa, Honolulu, HI 96822, United States of America

E-mail: wbi@uab.edu

Received 10 December 2023, revised 28 January 2024
Accepted for publication 15 March 2024
Published 27 March 2024

Abstract

Dirac materials offer exciting opportunities to explore low-energy carrier dynamics and novel physical phenomena, especially their interaction with magnetism. In this context, this work focuses on studies of pressure control on the magnetic state of $EuMnBi_2$, a representative magnetic Dirac semimetal, through time-domain synchrotron Mössbauer spectroscopy in ^{151}Eu. Contrary to the previous report that the antiferromagnetic order is suppressed by pressure above 4 GPa, we have observed robust magnetic order up to 33.1 GPa. Synchrotron-based x-ray diffraction experiment on a pure $EuMnBi_2$ sample shows that the tetragonal crystal lattice remains stable up to at least 31.7 GPa.

Keywords: Dirac semimetal, high pressure, crystal structure, magnetism

1. Introduction

Dirac materials, characterized by low-energy fermionic excitations behaving as massless Dirac particles, find potential application in electronic systems [1–3]. For exploring novel topological materials, magnetic Dirac materials with a layered structure comprising an insulating block layer and conducting Dirac/Weyl fermion layer appear to be promising for the possibility of manipulating the fermions through control of magnetic order under external stimuli such as magnetic field [4], chemical substitution [5], or pressure [6]. The layered material $AMnX_2$ (A: alkaline earth and rare-earth ions, X: Sb, Bi) [7–20] could implement the block-layer concept for Dirac/Weyl semimetals as $AMnX_2$ consists of an alternating arrangement of the X^- square net layer hosting quasi 2D Dirac fermions [21], and the insulating A^{2+}-Mn^{2+}-X^{3-} block layer [5].

Among the $AMnX_2$ materials, the initial focus turned toward $SrMnBi_2$ [6–8] for its manifestation of spin-degenerate quasi-2D Dirac bands observable along the Γ-M line [22]. In $SrMnBi_2$, the antiferromagnetic (AFM) order within the Mn layer seems to exert minimal impact on the Dirac fermion, while in $EuMnBi_2$, with the substitution of nonmagnetic Sr by magnetic Eu, high-field transport measurements indicate a

* Author to whom any correspondence should be addressed.

robust influence of the AFM order from the Eu layers [23], on quantum transport and the Dirac band due to strong exchange interactions [4].

$EuMnBi_2$ crystallizes in a tetragonal structure (space group $I4/mmm$) consisting of a MnBi layer with edge-sharing $MnBi_4$ tetrahedrons and a Bi square net layer sandwiched by Eu atoms [13, 24]. The Eu layers demonstrate AFM ordering below the Néel temperature, $T_N = 22$ K, characterized by a ferromagnetic arrangement of Eu moments within the *ab* plane and a sequential alignment along the *c*-axis as up-up-down-down [13, 14, 24]. $EuMnBi_2$ stands out as a distinctive system within the $AMnBi_2$ family, where the transport characteristics and the Fermi surface are significantly impacted by the magnetism from the Eu sublattice. It was found that the interlayer conductivity, along with the extent of spin splitting, significantly relies on the magnetic arrangement of the Eu layers and this arrangement can be regulated using an external magnetic field [4]. The Quantum Hall effect was detected in the system with the field-induced reorientation of the Eu moment [14]. This reorientation led to a decrease in the interlayer coupling, effectively constraining the Dirac fermions within the individual 2D Bi layer. Additionally, the Fermi energy in $EuMnBi_2$ can be regulated through the partial substitution of Gd^{3+} for Eu^{2+} within the block layer [5]. These studies demonstrate the strong tunability of this system.

These findings motivate us to use pressure as a control parameter and investigate the impact on the magnetic state, which provides the foundation for the magnetic control of electronic structure. Earlier electronic transport study indicates that the application of pressure initially enhances the T_N of Eu ions up to 4 GPa, beyond which the magnetic order is suppressed [25]. Under further compression to 6 GPa, another low-temperature transition of a different nature was observed. It was proposed that this transition is linked to temperature-induced valence transition from Eu^{2+} towards Eu^{3+}. Furthermore, x-ray absorption spectroscopy (XAS) studies up to 28 GPa provide evidence for divalent toward trivalent transition above 7 GPa without structural transformation. The valence transition is concurrent with Fermi surface modification suggested by Hall measurements. However, the sample used in this study contains a significant amount of Bi metal and an unidentified impurity phase. This necessitates further careful investigation into the magnetic and electronic states of this important material.

In this work, we have carefully analyzed the magnetism of Eu sublattice and crystal structure using a pure $EuMnBi_2$ sample under quasihydrostatic pressure using time-domain synchrotron Mössbauer spectroscopy (SMS) in ^{151}Eu and synchrotron x-ray diffraction (XRD) techniques up to 33.1 GPa and 31.7 GPa, respectively. Our experiments show that the magnetic ordering temperature (T_o) rises monotonically with increasing pressure and the magnetic order survives up to 33.1 GPa, contrary to the previous findings [25]. In addition, the tetragonal crystal lattice remains stable under compression up to at least 31.7 GPa.

2. Experimental methods

Single crystals of $EuMnBi_2$ were grown by the Bi self-flux method. Reactants included elemental Eu pieces (Alfa Aesar, sublimed dendritic, 99.9%), Mn pieces (Alfa Aesar, 99.9%), and Bi chunks (Alfa Aesar, 99.99%). The three metals were mixed in the ratio of Eu/Mn/Bi = 1:1:15, placed in an alumina crucible, and subsequently sealed in an evacuated silica tube ($<10^{-5}$ torr) with a sample mass of $\sim$3 g. The sample was heated up to 1050 °C at a rate of 60 °C h^{-1} and kept at 1050 °C for 10 hours. Then the sample was cooled to 850 °C at a rate of 100 °C h^{-1}, and finally, slowly cooled to 400 °C at a rate of 3 °C h^{-1}. The samples were then centrifuged to remove the excess Bi flux. Plate-like single crystals with a typical size of $\sim 3 \times 3 \times 1$ mm^3 were obtained. The crystal structure was determined using an XtaLAB Synergy-S single crystal x-ray diffractometer, equipped with Mo K_α radiation ($\lambda = 0.710\,73$ Å) with an ω of 2.0° per scan and an exposure time of 10 s per frame. A SHELXTL package with the direct methods and full-matrix least-squares on the F^2 model was used to determine the crystal structure [26, 27].

The magnetic state of $EuMnBi_2$ was probed under high pressure using ^{151}Eu SMS. Mössbauer spectroscopy under high-pressure sample environment is more feasible at the third-generation synchrotron sources compared to the conventional method using radioactive sources, due to the enhanced brilliance and compact size of the x-ray beams. Therefore, SMS is frequently employed in high-pressure magnetic research [28–32]. In conventional Mössbauer spectroscopy using a radioactive source, the Doppler effect modulates the source energy for energy-dependent absorption, whereas in time-domain SMS experiments, synchrotron radiation with an energy linewidth of $\sim$1 meV is used to coherently excite nuclear transitions and probe the hyperfine interactions from the reemitted radiation in time domain. Particularly, the 7/2 $\rightarrow$ 5/2 $M1$ nuclear transition at 21.54 keV in ^{151}Eu with half life of 9.5 ns is well suited for synchrotron radiation studies [33]. The substantial 48% natural abundance of the ^{151}Eu isotope allows for the use of samples with natural isotope abundance. The experiments were conducted at the Beamline 3ID of the Advanced Photon Source (APS), Argonne National Laboratory (ANL). The time-domain data was collected using 24-bunch timing mode with 153 ns intervals between the consecutive electron bunches. A miniature diamond anvil cell (DAC) and a compatible helium flow cryostat were utilized to achieve high pressure and low temperature [34]. A single crystal sample was loaded in the DAC. Pressures were determined *in situ* based on the shift of the ruby $R1$ fluorescence line [35]. Neon gas served as a quasihydrostatic pressure-transmitting medium. CONUSS program was used to analyze the SMS data and derive hyperfine parameters such as magnetic hyperfine field (B_{hf}) and electric quadrupole interaction (Δ) [36].

To investigate the crystal structure under high pressures, angle-dispersive synchrotron XRD experiments were carried out at room temperature at the 13BM-C beamline (PX^2) of the

APS, ANL [37]. X-rays with a wavelength of 0.434 Å were employed. To generate pressures up to 32 GPa, a BX-90 DAC equipped with Boehler-Almax anvils of 400 μm diameter culet size was used. A Re gasket, preindented to 76 μm with a 210 μm hole drilled using electrical discharge machining, was positioned between the anvils to create a sample chamber. A powder sample was loaded in the chamber with two ruby balls serving as an *in situ* pressure marker [35]. Neon gas was used as a pressure-transmitting medium. The two-dimensional diffraction images were integrated using the DIOPTAS software [38]. High-pressure XRD data were fitted using Le Bail method in GSAS-II [39].

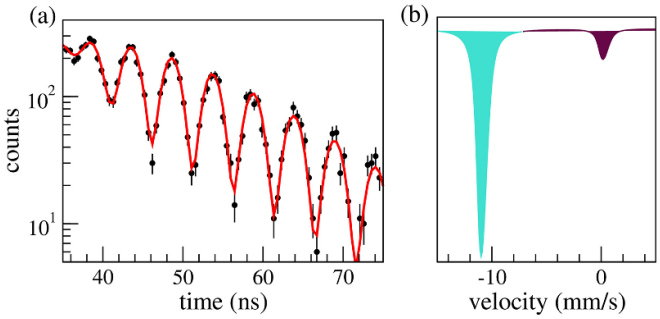

Figure 1. (a) Time-domain ^{151}Eu SMS spectrum in $EuMnBi_2$ at 0.6 GPa along with EuF_3 as a reference at ambient conditions. (b) The corresponding simulated energy-domain spectrum. Shaded blue line represents the resonant absorption from $EuMnBi_2$ and shaded brown line is from the reference sample EuF_3.

3. Results and discussion

The substantial difference in isomer shift values between the Eu^{2+} and Eu^{3+} valence states renders it a valuable parameter for providing information on the valence state of Eu ions [29, 40]. The isomer shift (δ) of ^{151}Eu in $EuMnBi_2$ at 0.6 GPa and room temperature was determined from the SMS spectrum taken together with a trivalent EuF_3 (δ:0 mm s^{-1}) as a reference sample. Figure 1 shows the time-domain spectrum as well as the simulated Mössbauer spectrum in the energy domain based on the parameters obtained from fitting the experimental data. δ is derived to be -11.3 mm s^{-1}, a typical value for Eu^{2+}. This value is also comparable to the reported -11.4 mm s^{-1} (relative to the $^{151}SmF_3$ source) in a sister compound $EuMnSb_2$ [41].

Representative SMS spectra in ^{151}Eu from $EuMnBi_2$ at different temperatures and pressures are displayed in figure 2. B_{hf} and Δ, along with the effective sample thickness, served as fitting variables. For $4f^7$ ions, the magnetic hyperfine field arises due to contributions from core electron polarization, conduction electron polarization by ions, and neighboring atoms [28, 42]. In the presence of magnetic order, Zeeman splitting of nuclear levels leads to quantum oscillations in the SMS spectrum, with additional beating frequency from quadrupole interaction. At constant pressure, the oscillation frequency decreases as the temperature rises due to a reduction in the B_{hf} strength. The oscillations disappear when the sample is warmed up to the paramagnetic phase. At 1.6 GPa and 13.2 K B_{hf} is 25.98(3) T, consistent with the magnetic hyperfine field observed in other divalent Eu-based compounds [41, 43, 44]. At 1.6 GPa T_o lies between 23 K and 37 K. Above T_o no sizable quadrupole interaction is resolved. At pressure higher than 8.6 GPa, T_o increases to a temperature above 35 K. At the lowest temperature ($\sim$13 K), the oscillation frequency increases as pressure is raised from 1.6 GPa to 33.1 GPa, attributed to increasing B_{hf} which leads to nuclear Zeeman splitting in larger energy range. This is also demonstrated in the simulated energy-domain spectra (see figure 2(b)) based on the fitting parameters to the experiment data. The B_{hf} values at various temperatures and pressures are summarized in figure 3. At around 13 K, B_{hf} increases monotonically with pressure.

Table 1 tabulates the derived hyperfine parameters. The main determinant of Δ is the electric field gradient (EFG) at the nucleus, which arises from lattice charge distribution and incompletely filled electronic shells. In the case of Eu^{2+}, the half-filled $4f$ shell conforms to Hund's rule, rendering the isotropic electronic ground state ($^8S_{7/2}$) and yielding no electronic contribution to Δ due to zero total angular momentum [45]. Consequently, Δ values predominantly mirror the EFG originating from the lattice effects. Note that in the magnetic phase, a small Δ value is needed to fit the SMS data.

The tetragonal crystal structure (*I*4/*mmm*) of $EuMnBi_2$ was confirmed at ambient conditions from single crystal XRD with Mo radiation ($\lambda = 0.71073$ Å). The lattice parameters agree well with the reported values in [13]. The atomic occupancies were checked carefully and no vacancies were observed from the XRD data. The detailed crystal structure information is tabulated in table 2.

The crystal structure of $EuMnBi_2$ was investigated under pressures up to 31.7 GPa using synchrotron XRD. As shown in figure 4(a), the XRD data can be indexed with the tetragonal space group *I*4/*mmm* up to at least 31.7 GPa, indicating the stable tetragonal lattice in this pressure range. The XRD data also confirms the purity of the sample. The lattice parameters and volume under pressure are displayed in figures (b)–(e). Analyzing the pressure-volume data with the third-order Birch–Murnaghan equation of state yields the bulk modulus $B_0 = 36.7(3)$ GPa, its pressure derivative $B_0' = 4.32(5)$, and zero-pressure volume $V_0 = 457.87(6)$ Å^3. The B_0 value is slightly lower than the reported value of 41.8 GPa [25]. This small discrepancy may originate from the less hydrostatic pressure medium used in the earlier study.

Our high-pressure SMS measurements show that the magnetic ordering temperature in $EuMnBi_2$ lies above 25 K at 3 GPa, in agreement with the earlier report that T_N increases continuously to 31 K at 3.9 GPa. This initial increase may be attributed to the enhanced Ruderman–Kittel–Kasuya–Yosida exchange interaction, primarily the intralayer exchange coupling due to the smaller Eu–Eu distance within the *ab*-plane than along the *c*-axis. At higher pressure, our SMS data show that at 20.5 GPa the T_o lies higher than 35 K and the magnetic order persists up to 33.1 GPa, contrary to the report from Susilo *et al* that T_N is suppressed above 4 GPa based on electrical resistivity measurements [25]. It is noted that

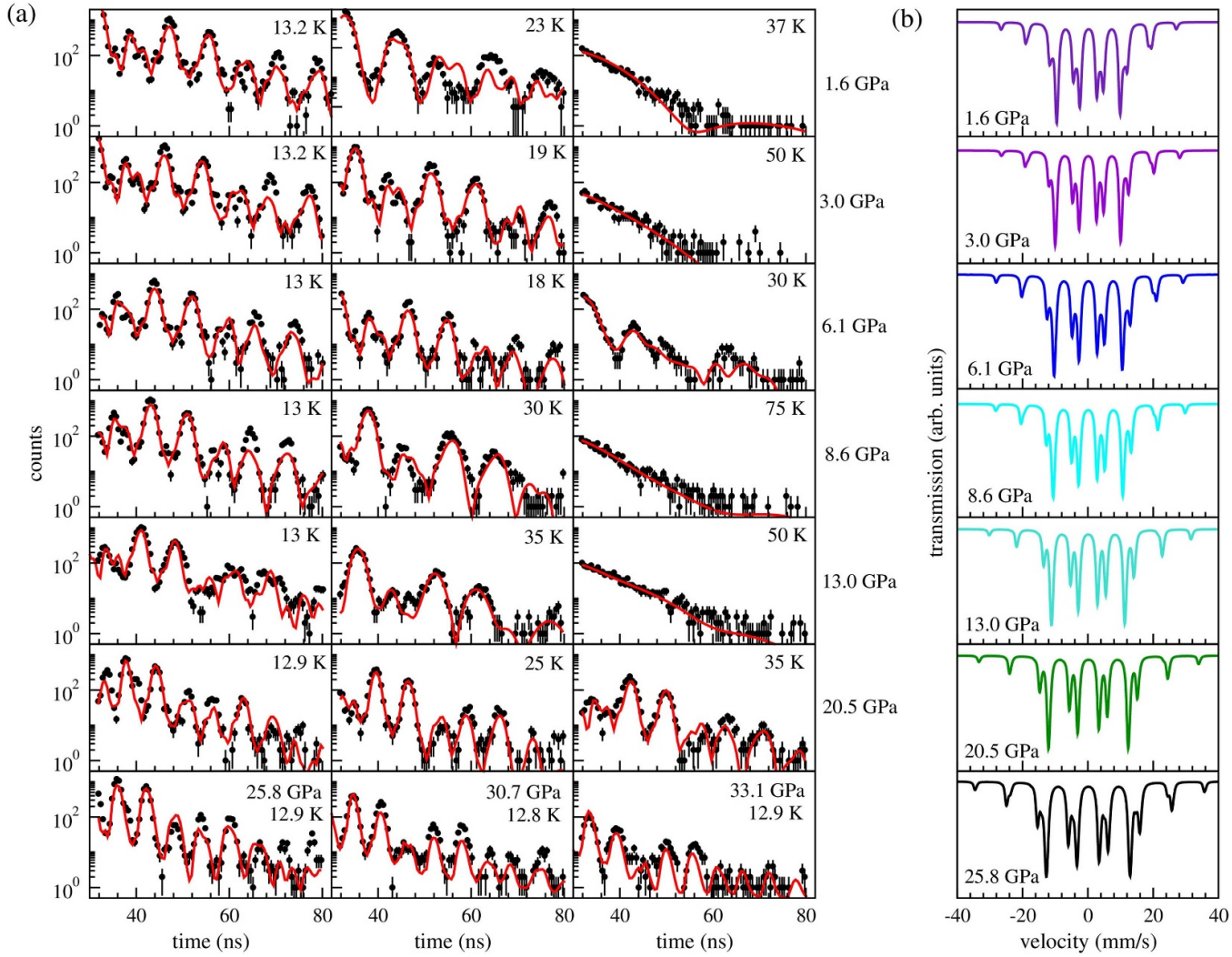

Figure 2. (a) Time-domain ^{151}Eu SMS spectra in $EuMnBi_2$. The black solid circles represent the experimental data and red lines correspond to the fits from the CONUSS program. (b) Simulated Mössbauer spectra in energy domain corresponding to the fits for the time-domain data in (a) at the lowest temperature (∼13 (K) achieved at each pressures.

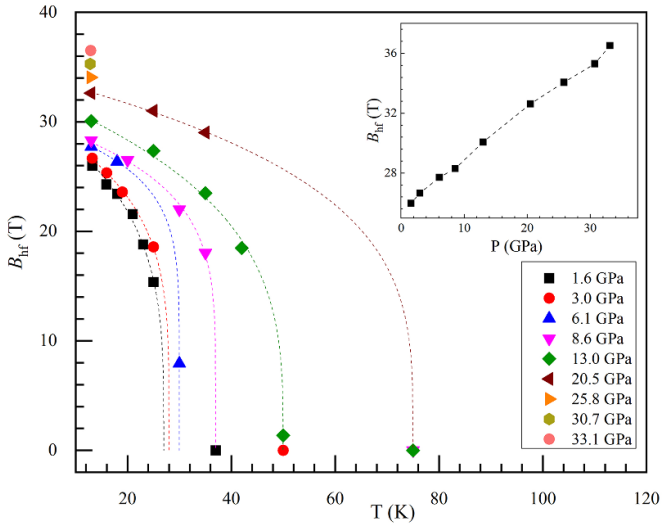

Figure 3. Magnetic hyperfine field of ^{151}Eu in $EuMnBi_2$ as a function of temperature at various pressures. Error bars are smaller than the symbol size. The dashed lines serve as a guide to the eye. The plot of B_{hf} as a function of pressure around 13 K is shown in inset.

Table 1. List of magnetic hyperfine field (B_{hf}) and electric quadrupole interaction (Δ) of ^{151}Eu in $EuMnBi_2$ at high pressures and various temperatures. The error bars are generated from the fitting uncertainties in CONUSS.

P (GPa)	T (K)	B_{hf} (T)	Δ (mm/s)
1.6	13.2	25.98(3)	4.0(1)
	15.9	24.29(3)	3.7(1)
	18	23.42(2)	3.8(2)
	21	21.57(1)	3.3(1)
	23	18.80(5)	3.0(2)
	25	15.36(4)	2.6(1)
	37	0	1.2(1)
3	13.2	26.67(4)	4.3(1)
	16	25.33(5)	3.7(2)
	19	23.58(4)	3.0(2)
	25	18.56(6)	3.3(2)
	50	0	0
6.1	13	27.72(4)	3.8(2)
	18	26.37(5)	4.2(2)
	30	7.92(3)	4.3(7)
8.6	13	28.30(5)	4.3(2)
	20	26.52(4)	3.6(2)
	30	22.0(5)	3.9(2)
	35	18.04(5)	4.1(1)
	75	0	0
13	13	30.07(6)	6.0(2)
	25	27.34(1)	5.5(3)
	35	23.50(6)	5.1(2)
	42	18.48(8)	2.1(2)
	50	1.36(3)	0
	75	0	0
	120	0	0
20.5	12.9	32.62(5)	5.2(3)
	25	31.01(3)	5.3(2)
	35	29.03(4)	5.3(1)
25.8	12.9	34.06(6)	4.8(3)
30.7	12.8	35.30(3)	4.7(4)
33.1	12.9	36.51(7)	2.7(9)

Mössbauer effect is a sensitive probe for detecting magnetic transition, while in resistivity measurements other phenomena may obscure the signature of magnetic order and it becomes challenging to interpret the data on magnetic state with full confidence.

In Eu-based magnetic intermetallic compounds, pressure typically has the effect of reducing the magnetic transition temperature and/or magnetic moment [46]. This is because a valence transition from magnetic Eu^{2+} ($J = 7/2$) to nonmagnetic Eu^{3+} ($J = 0$) is anticipated under high pressure, given that the ionic radius of Eu^{3+} is smaller than that of Eu^{2+}. This valence transition has been observed in many compounds such as parent and doped $EuFe_2As_2$ [43, 47], $Eu(Fe_{1-x}Ni_x)As_2$ [29], and $EuRh_2Si_2$ [48]. Similarly, in $EuMnBi_2$ high-pressure XAS measurements at Eu L_3 edge indicate a large increase in Eu mean valence by $\sim$0.4 at 27 GPa [25]. It is surprising to maintain the magnetic order up to 33.1 GPa with such a significant valence increase. To understand the robust magnetism in this important material, further theoretical investigations are desired.

Table 2. Single crystal XRD refinement and atomic coordinates and equivalent isotropic displacement parameters for $EuMnBi_2$ at ambient conditions. U_{eq} is defined as one-third of the trace of the orthogonalized U_{ij} tensor ($Å^2$).

Space group						*I*4/*mmm*
a (Å)						4.5510(7)
c (Å)						22.560(6)
V (A^3)						467.1(2)
θ range (°)						3.613–25.102
# of reflections; R_{int}						1072; 0.1429
# of independent reflections						161
# of parameters						13
R_1; ωR_2 ($I>2\delta(I)$)						0.1428; 0.3045
Goodness of fit (GOF)						1.085
Atom	Wyck.	*x*	*y*	*z*	Occ.	U_{eq}
Eu	4e	0	0	0.1124(2)	1	0.036(3)
Mn	4d	0	0.5	0.25	1	0.032(2)
Bi1	4c	0	0.5	0	1	0.035(3)
Bi2	4e	0	0	0.3282(3)	1	0.032(3)

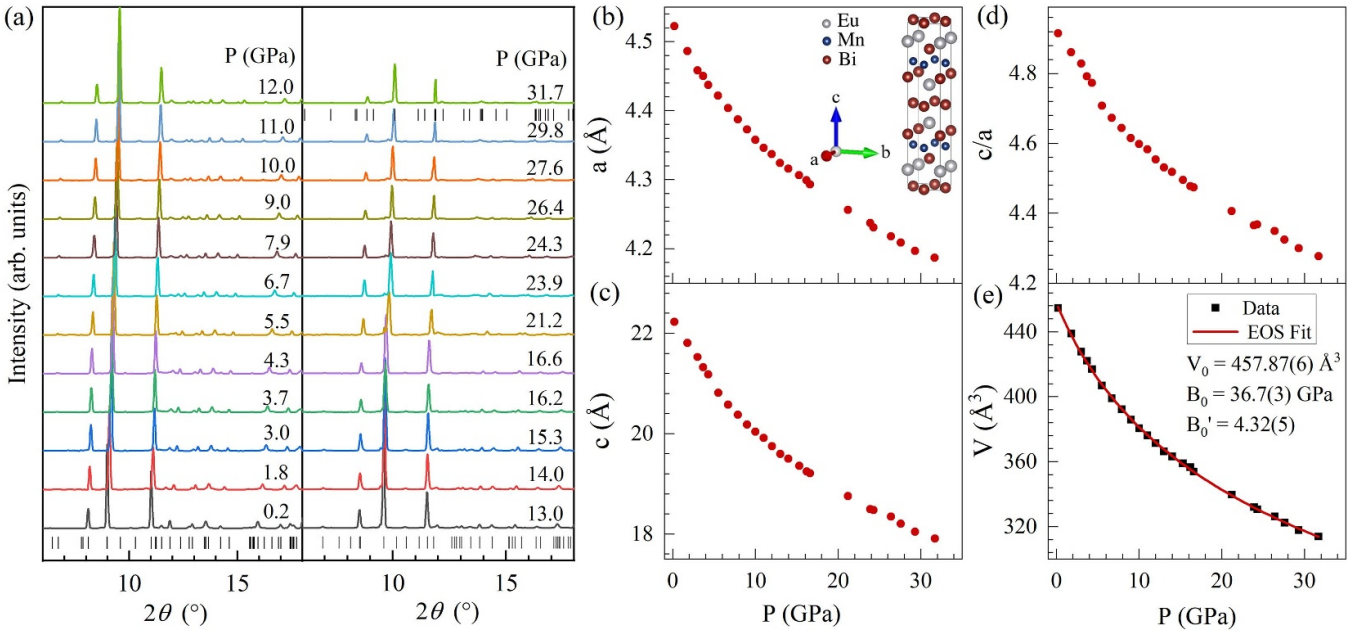

Figure 4. (a) XRD spectra of $EuMnBi_2$ under pressure up to 31.7 GPa. In this pressure range, the Bragg peaks can be indexed with the *I*4/*mmm* space group. (b)–(e) Lattice parameters and unit cell volume under pressure. Error bars are smaller than the symbol size. The inset in (b) shows the crystal structure of $EuMnBi_2$.

4. Conclusion

In this study, we investigated the magnetic properties and crystal structure of $EuMnBi_2$ under quasihydrostatic pressure conditions. Using time-domain SMS in ^{151}Eu, we have found that the magnetic order of Eu sublattice persists up to 33.1 GPa with T_o higher than 35 K at 20.5 GPa. These results are in sharp contrast to the previous claim of suppression of magnetic order above 4 GPa based on electrical resistivity studies. Our synchrotron XRD experiment on a high-quality $EuMnBi_2$ sample shows that the ambient tetragonal structure remains stable up to pressure as high as 31.7 GPa. Our findings highlight that high pressure serves as an effective approach to enhance the magnetic exchange interaction. The experimental data provide foundation for further experimental as well as theoretical studies.

Data availability statement

The data cannot be made publicly available upon publication because they are not available in a format that is sufficiently accessible or reusable by other researchers. The data that support the findings of this study are available upon reasonable request from the authors.

Acknowledgments

This work was supported by the National Science Foundation (NSF) Award No. OIA-2033131. G C J acknowledges the financial support from the Alabama Graduate Research Scholars Program (GRSP) funded through the Alabama Commission for Higher Education and administered by the Alabama EPSCoR. W X was supported by U.S. DOE-BES under Contract DE-SC0023648. This research used resources of the Advanced Photon Source, a U.S. DOE Office of Science user facility operated for the DOE Office of Science by Argonne National Laboratory under Contract No. DE-AC02-06CH11357. Uses of the COMPRES-GSECARS gas loading system and the PX^2 program were supported by COMPRES under NSF Grant EAR-1661511 and GSECARS through NSF Grant EAR-1634415. B L acknowledges the support from COMPRES. We are grateful to Haozhe Wang's analysis of the single crystal diffraction data.

ORCID iDs

Weiwei Xie https://orcid.org/0000-0002-5500-8195
Wenli Bi https://orcid.org/0000-0002-2067-6556

References

[1] Wehling T O, Black-Schaffer A M and Balatsky A V 2014 Dirac materials *Adv. Phys.* **63** 1–76
[2] Vafek O and Vishwanath A 2014 Dirac fermions in solids: from high-T_c cuprates and graphene to topological insulators and Weyl semimetals *Annu. Rev. Condens. Matter Phys.* **5** 83–112
[3] Cayssol J 2013 Introduction to Dirac materials and topological insulators *C. R. Phys.* **14** 760–78
[4] Sakai H 2022 High-field studies on layered magnetic and polar Dirac metals: novel quantum transport phenomena coupled with spin-valley degrees of freedom *J. Phys. Soc. Japan* **91** 101001
[5] Tsuruda K, Nakagawa K, Ochi M, Kuroki K, Tokunaga M, Murakawa H, Hanasaki N and Sakai H 2021 Enhancing thermopower and Nernst signal of high-mobility Dirac carriers by Fermi level tuning in the layered magnet $EuMnBi_2$ *Adv. Funct. Mater.* **31** 2102275
[6] Farhan M A, Lee G and Shim J H 2014 $AEMnSb_2$ (AE = Sr, Ba): a new class of Dirac materials *J. Condens. Matter Phys.* **26** 042201
[7] Park J *et al* 2011 Anisotropic Dirac fermions in a Bi square net of $SrMnBi_2$ *Phys. Rev. Lett.* **107** 126402
[8] Wang J K, Zhao L L, Yin Q, Kotliar G, Kim M S, Aronson M C and Morosan E 2011 Layered transition-metal pnictide $SrMnBi_2$ with metallic blocking layer *Phys. Rev.* B **84** 064428
[9] Wang K, Graf D, Lei H, Tozer S W and Petrovic C 2011 Quantum transport of two-dimensional Dirac fermions in $SrMnBi_2$ *Phys. Rev.* B **84** 220401
[10] Jia L L *et al* 2014 Observation of well-defined quasiparticles at a wide energy range in a quasi-two-dimensional system *Phys. Rev.* B **90** 035133
[11] Li L, Wang K, Graf D, Wang L, Wang A and Petrovic C 2016 Electron-hole asymmetry, Diracfermions and quantum magnetoresistance in $BaMnBi_2$ *Phys. Rev.* B **93** 115141
[12] Wang Y Y, Yu Q H and Xia T L 2016 Large linear magnetoresistance in a new Dirac material $BaMnBi_2$ *Chin. Phys.* B **25** 107503
[13] May A F, McGuire M A and Sales B C 2014 Effect of Eu magnetism on the electronic properties of the candidate Dirac material $EuMnBi_2$ *Phys. Rev.* B **90** 075109
[14] Masuda H *et al* 2016 Quantum Hall effect in a bulk antiferromagnet $EuMnBi_2$ with magnetically confined two-dimensional Dirac fermions *Sci. Adv.* **2** e1501117
[15] Wang A, Zaliznyak I, Ren W, Wu L, Graf D, Garlea V O, Warren J B, Bozin E, Zhu Y and Petrovic C 2016 Magnetotransport study of Dirac fermions in $YbMnBi_2$ antiferromagnet *Phys. Rev.* B **94** 165161
[16] Liu J *et al* 2016 Nearly massless Dirac fermions hosted by Sb square net in $BaMnSb_2$ *Sci. Rep.* **6** 30525
[17] Huang S, Kim J, Shelton W A, Plummer E W and Jin R 2017 Nontrivial Berry phase in magnetic $BaMnSb_2$ semimetal *Proc. Natl Acad. Sci. USA* **114** 6256–61
[18] Sakai H *et al* 2020 Bulk quantum Hall effect of spin-valley coupled Dirac fermions in the polar antiferromagnet $BaMnSb_2$ *Phys. Rev.* B **101** 081104
[19] Zhang A *et al* 2016 Interplay of Dirac electrons and magnetism in $CaMnBi_2$ and $SrMnBi_2$ *Nat. Commun.* **7** 13833
[20] Graf K W, Wang L, Lei H, Tozer S W and Petrovic C 2012 Two-dimensional Dirac fermions and quantum magnetoresistance in $CaMnBi_2$ *Phys. Rev.* B **85** 041101
[21] Lee G, Farhan M A, Kim J S and Shim J H 2013 Anisotropic Dirac electronic structures of $AMnBi_2$(A= Sr, Ca) *Phys. Rev.* B **87** 245104
[22] Feng Y *et al* 2014 Strong anisotropy of Dirac cones in $SrMnBi_2$ and $CaMnBi_2$ revealed by angle-resolved photoemission spectroscopy *Sci. Rep.* **4** 5385
[23] Nishiyama H *et al* 2021 Variation of charge dynamics upon antiferromagnetic transitions in the Dirac semimetal $EuMnBi_2$ *Phys. Rev.* B **104** 115111
[24] Zhu F *et al* 2020 Magnetic structures, spin-flop transition and coupling of Eu and Mnmagnetism in the Dirac semimetal $EuMnBi_2$ *Phys. Rev. Res.* **2** 043100
[25] Susilo R A *et al* 2021 Impacts of pressure to the structural, electronic and magnetic properties of Dirac semimetal $EuMnBi_2$ *Phys. Rev. Res.* **3** 043028
[26] George M S 2015 *SHELXT*-Integrated space-group and crystal-structure determination *Acta Cryst.* A **71** 3–8
[27] George M S 2015 Crystal structure refinement with SHELXL *Acta Cryst.* C **71** 3–8
[28] Bi W *et al* 2016 Magnetism of europium under extreme pressures *Phys. Rev.* B **93** 184424
[29] Bi W *et al* 2021 Microscopic phase diagram of $Eu(Fe_{1-x}Ni_x)As_2$ (x = 0,0.04) under pressure *Phys. Rev.* B **103** 195135
[30] Bi W *et al* 2022 Drastic enhancement of magnetic critical temperature and amorphization in topological magnet $EuSn_2P_2$ under pressure *npj Quantum Mater.* **7** 1–8
[31] Sergueev I *et al* 2013 Hyperfine splitting and room-temperature ferromagnetism of Ni at multimegabar pressure *Phys. Rev. Lett.* **111** 157601
[32] Jose G C *et al* 2023 Evolution of magnetism, valence and crystal lattice in $EuCd_2As_2$ under pressure *Phys. Rev.* B **107** 245121
[33] Leupold O, Pollmann J, Gerdau E, Rüter H D, Faigel G, Tegze M, Bortel G, Rüffer R, Chumakov A I and Baron A Q 1996 Nuclear resonance scattering of synchrotron radiation at the 21.5 keV resonance of ^{151}Eu *Europhys. Lett.* **35** 671
[34] Zhao J Y, Bi W, Sinogeikin S, Hu M Y, Alp E E, Wang X C, Jin C Q and Lin J F 2017 A compact membrane-driven diamond anvil cell and cryostat system for nuclear resonant scattering at high pressure and low temperature *Rev. Sci. Instrum.* **88** 125109

[35] Dewaele A, Torrent M, Loubeyre P and Mezouar M 2008 Compression curves of transition metals in the Mbar range: experiments and projector augmented-wave calculations *Phys. Rev.* B **78** 104102
[36] Sturhahn W 2000 Conuss and phoenix: evaluation of nuclear resonant scattering data *Hyperfine Interact.* **125** 149–72
[37] Zhang D, Dera P K, Eng P J, Stubbs J E, Zhang J S, Prakapenka V B and Rivers M L 2017 High pressure single crystal diffraction at PX^2 *J. Vis. Exp.* **119** 54660
[38] Prescher C and Prakapenka V B 2015 DIOPTAS:a program for reduction of two-dimensional x-ray diffraction data and data exploration *High Press. Res.* **35** 223–30
[39] Toby B H and Von Dreele R B 2013 GSAS-II: the genesis of a modern open-source all purpose crystallography software package *J. Appl. Crystallogr.* **46** 544–9
[40] Souza-Neto N M, Zhao J, Alp E E, Shen G, Sinogeikin S V, Lapertot G and Haskel D 2012 Reentrant valence transition in EuO at high pressures: beyond the bond-valence model *Phys. Rev. Lett.* **109** 026403
[41] Wilde J M *et al* 2022 Canted antiferromagnetic phases in the candidate layered Weyl material $EuMnSb_2$ *Phys. Rev.* B **106** 024420
[42] Nowik I, Dunlap B D and Wernick J H 1973 Contributions to the hyperfine field in europium intermetallics *Phys. Rev.* B **8** 238–41
[43] Nix Z, Zhao J, Alp E E, Xiao Y, Zhang D, Cao G H, Vohra Y K and Bi W 2022 Pressure effect on magnetism and valence in ferromagnetic superconductor $Eu(Fe_{0.75}Ru_{0.25})_2As_2$ *J. Phys.: Condens. Matter* **34** 415601
[44] Nowik I, Felner I, Ren Z, Cao G H and Xu Z A 2011 ^{57}Fe and ^{151}Eu Mössbauer spectroscopy and magnetization studies of $Eu(Fe_{0.89}Co_{0.11})_2As_2$ and $Eu(Fe_{0.9}Ni_{0.1})_2As_2$ *New J. Phys.* **13** 023033
[45] Kalvius G M, Shenoy G K, Ehnholm G J, Katila T E, Lounasmaa O V and Reivari P 1969 Quadrupole Moment of the 21.6-keV State of ^{151}Eu *Phys. Rev.* **187** 1503–5
[46] Ōnuki Y *et al* 2017 Divalent, trivalent and heavy fermion states in Eu compounds *Phil. Mag.* **97** 3399–414
[47] Matsubayashi K *et al* 2011 Pressure-induced changes in the magnetic and valence state of $EuFe_2As_2$ *Phys. Rev.* B **84** 024502
[48] Mitsuda A, Hamano S, Araoka N, Yayama H and Wada H 2012 Pressure-induced valence transition in antiferromagnet $EuRh_2Si_2$ *J. Phys. Soc. Japan* **81** 023709